Electronic Supplementary Information (ESI)

Non-flammable, dilute, and hydrous organic electrolytes for reversible Zn batteries

Guoqiang Ma,‡[a] Licheng Miao,‡[c] Wentao Yuan,[a] Kaiyue Qiu,[a] Mengyu Liu,[a] Xueyu Nie,[a] Yang Dong,[b] Ning Zhang,*[a] and Fangyi Cheng*[bd]

[a] College of Chemistry & Environmental Science, Key Laboratory of Analytical Science and Technology of Hebei Province, Hebei University, Baoding 071002, P. R. China. E-mail: ningzhang@hbu.edu.cn

[b] Key Laboratory of Advanced Energy Materials Chemistry (Ministry of Education), College of Chemistry, Nankai University, Tianjin 300071, P. R. China. E-mail: fycheng@nankai.edu.cn

[c] College of Physics and Optoelectronic Engineering, Shenzhen University, Shenzhen 518060, P. R. China.

[d] Haihe Laboratory of Chemical Transformation, Tianjin 300071, P. R. China.

‡ These authors contributed equally to this work.

Experimental Section

Preparation of electrolytes. The hydrated Zn-salts in terms of $Zn(ClO_4)_2·6H_2O$, $Zn(NO_3)_2·6H_2O$, $Zn(Ac)_2·2H_2O$, and $ZnSO_4·7H_2O$ and typical organic solvents in terms of ethylene glycol (EG), acetonitrile (AN), trimethyl phosphate (TMP), dimethyl carbonate (DMC), and 1,2-dimethoxyethane (DME) were purchased from *Aladdin Chemicals*. The hydrous organic electrolytes were prepared by directly dissolving the hydrated Zn-salt in a specific organic solvent at room temperature. For example, the $Zn(ClO_4)_2·6H_2O$/TMP electrolytes with various concentrations (e.g., 0.2, 0.5, 1, and 2 mol/kg (m)) were prepared by dissolving the desired amount of $Zn(ClO_4)_2·6H_2O$ salt in TMP. The saturated concentration of $Zn(ClO_4)_2·6H_2O$ in TMP is around 2.2 m. For comparison, 0.5 m $Zn(ClO_4)_2·6H_2O$ aqueous electrolyte was also prepared.

Synthesis of $Zn_{0.13}V_2O_5·nH_2O$ cathode material. The preparation of $Zn_{0.13}V_2O_5·nH_2O$ (ZVO) powder is according to a previous report.[S1] In detail, 365 mg V_2O_5, 2 mL H_2O_2, and 30 mL H_2O were mixed to obtain a solution. After stirring for 30 min, 75 mg $Zn(NO_3)_2$ and 800 mg polyethylene glycol were added into the above solution followed by continuously stirring for 30 min. Afterward, the mixture was sealed in a 50 mL Teflon autoclave and heated at 120 °C for 12 h. The resulting precipitation of $Zn_{0.13}V_2O_5·nH_2O$ was collected and washed thoroughly using water and ethanol, and then vacuum dried at 80 °C for 12 h. The $Zn_xV_2O_5·nH_2O$ cathode was prepared by blending the slurry mixture of active materials, Super P carbon, and carboxymethyl cellulose in a mass ratio of 7:2:1 using water as the solvent onto a Ti foil, and then was dried at 60 °C for 10 h under vacuum. The as-prepared electrode was cut into round slices with a typical mass loading of ~2-3 mg cm^{-2}.

Preparation of high mass loading ZVO cathode. The ZVO cathode with high mass loading was prepared by a vacuum infiltration method. The mixture of CNT suspension and ZVO powder (weight ratio, 2:8) was added into *N*,*N*-Dimethylformamide solvent and sonicated for 2 h and then vacuum-infiltrated. The free-standing cathode was dried at 60 °C for 10 h.

Characterization. Raman spectra and FTIR spectra of the electrolytes were performed on a Horiba HR-Evolution Raman microscope (using 532 nm excitation) and a Nicolet iS10 spectrometer (Thermo-Fisher Scientific), respectively. X-ray diffraction (XRD) patterns were collected on a Bruker D8 ADVANCE (Cu Kα radiation) at a scanning rate of 4° min^{-1}. Contact angle measurement was characterized on Dataphysics OCA15 optical contact angle system. The viscosity of electrolytes was obtained on an MDJ-5S viscometer at room temperature. Scanning electron microscopy (SEM) images were obtained on a scanning electron microscope (JEOL, JSM-7500F). XPS spectra were carried out on a ESCALAB 250Xi spectrometer (ThermoFisher). All of the binding energies were

referenced to the C 1s peak (284.8 eV). The *in-situ* characterization of Zn plating behavior on the Cu substrate in electrolytes was conducted on an optical microscope (ZEISS, AxioVert. A1) equipped with a digital camera. Thermogravimetric analysis (TGA) of electrolytes was performed on a Netzsch STA 449C thermal analyzer under N_2 atmosphere from 35 to 150 ^oC with a heating rate of 10 $^oC\ min^{-1}$.

Electrochemical Measurements. Electrochemical performances of half and full batteries were evaluated using CR-2032 coin-type cells. Glass fibre was used as the separator and the loading volume of electrolyte in each cell was 80 μL. The Coulombic efficiencies of Zn^{2+} plating/stripping in different electrolytes were measured using asymmetric Zn//Cu and Zn//Ti cells. The cycling stability of Zn electrode in different electrolytes was conducted using symmetric Zn//Zn cells. The thickness of Zn electrode was 50 μm. Charge/discharge of battery was tested on a LAND-CT2001A battery-testing instrument. The applied current density and specific capacity in the $Zn//Zn_{0.13}V_2O_5{\cdot}nH_2O$ full battery were calculated based on the cathode mass. The electrochemical impedance spectroscopy (with a frequency range from 100 mHz to 100 kHz) and cyclic voltammetry (CV) profiles were performed on the Solartron 1470E electrochemical workstation. The ionic conductivity (σ) of electrolytes was evaluated by the following equation: $\sigma = L/RA$, where R is the resistance according to the EIS measurement at 25 ^oC, L is the electrolyte thickness, and A is the contact area between electrode and electrolyte in the testing cell.

Computational details

Molecular dynamics simulations: We performed all-atom MD computer simulations of bulk electrolytes employing the GROMACS simulation package[S2]. The compositions of species for the MD simulations were provided in Table S1. The properties of electrolytes were scrutinized using AMBER03 force field.[S3] The force-field parameters of Zn^{2+}, ClO_4^-, and TMP were generated by ACPYPE, and they were in the built-in force-field parameters.[S4] The properties of H_2O were assessed using the extended simple point charge (SPC/E) model. Electrostatic interactions and Van der Waals (vdW) and were treated using the Particle-Mesh-Ewald (PME) and cut-off methods respectively with the cutoff radius of 10 Å. All the simulations were performed in the NpT ensemble with constant pressure (1.01 atm) and temperature (298.15 K) in a cubic box with periodic boundary conditions in all three Cartesian directions. Each system was initially equilibrated for 10 ns (5000000 steps, 2 fs per step). The Velocity-rescale thermostat and the Berendsen barostat were used to control the system temperature and pressure respectively in this stage. After the system was fully equilibrated, the production simulation ran for 10 ns (5000000 steps, 2 fs per step) to collect the data for statistical analysis. During the production simulation, the pressure was controlled by the Parrinello-

rahman barostat. The radial distribution functions (RDFs, g(r)) were calculated with the GROMACS built-in module. The coordination number (N(r)) and snapshots of MD simulation were performed by the VMD software.[S5]

Quantum chemistry calculations: Density functional theory (DFT) calculations were carried out using the Gaussian 16 software to calculate structures, binding energies (BE), and lowest unoccupied molecular orbitals (LUMO). All of the molecular structures were optimized at the theoretical level of B3LYP/6-31+g (d, p) for H, C, O, P, and Cl atoms, with the Zn atom using the SDD pseudo potential. Frequency calculations were performed at the same level to confirm each optimized structure being a stationary point. The BE is obtained by the following equation of BE = $E_{AB} – (E_A + E_B) - E_{BSSE}$, where E_{AB}, E_A, and E_B denote the total energies of the AB complexes, bare A, and bare B, respectively. E_{BSSE} is the basis set superposition error (BSSE) correction energy, which is used to correct the geometries and interaction energies in all the complexes.

The adsorption energy (E_{ads}) was carried out using Vienna Ab initio Simulation Package (VASP) within projector augmented wave (PAW) pseudopotentials for core electrons and Perdew-Burke-Ernzerhof form of the generalized-gradient approximation (PBE-GGA) for exchange and correlation functional. The cutoff for plane wave was set to 400 eV. The Brillouin zone integration was sampled using a Monkhorst-Pack special k-point mesh of Γ-centered 1 × 1 × 1 for all the structures. The convergence threshold for energy was set to 10^{-5} eV during ion relaxation, and the convergence thresholds for force was set to 0.035 eV·Å^{-1}. The adsorption energy (E_{ads}) is calculated as follows:

$$E_{ads} = E_{Zn(002)+adsorbent} – (E_{Zn(002)} + E_{adsorbent})$$

where $E_{Zn(002)+adsorbent}$, $E_{Zn(002)}$, and $E_{adsorbent}$ represent the total energies of the Zn(002) facet with the adsorbent (e.g., H_2O or TMP), bare Zn(002) facet, and bare adsorbent (e.g., H_2O or TMP), respectively.

Supplementary Figures and Tables

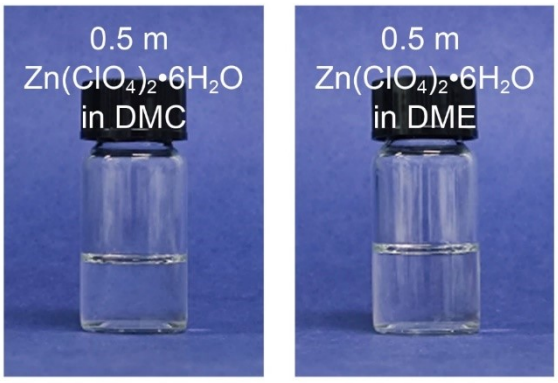

Fig. S1. Electrolyte digital photos of 0.5 m $Zn(ClO_4)_2 \cdot 6H_2O$ in DMC and 0.5 m $Zn(ClO_4)_2 \cdot 6H_2O$ in DME.

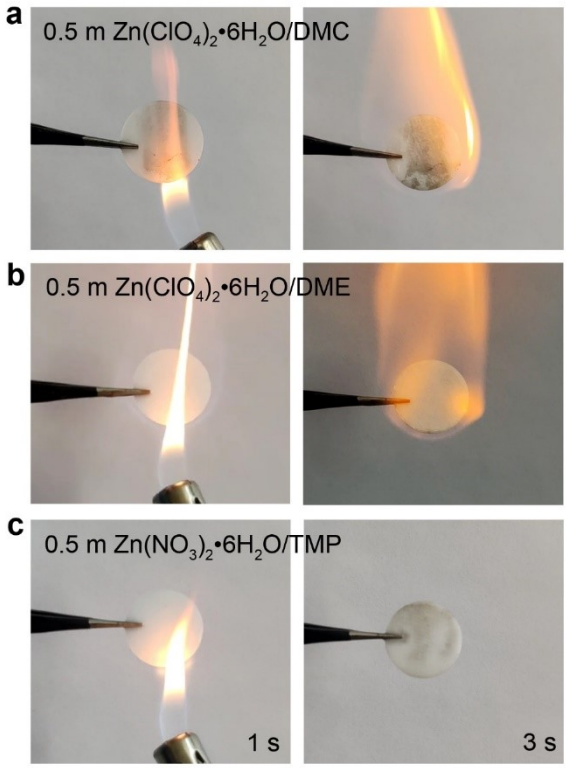

Fig. S2. Ignition tests of glass fiber separators saturated with electrolytes of (a) 0.5 m $Zn(ClO_4)_2 \cdot 6H_2O$ in DMC, (b) 0.5 m $Zn(ClO_4)_2 \cdot 6H_2O$ in DME, and (c) 0.5 m $Zn(NO_3)_2 \cdot 6H_2O$ in TMP.

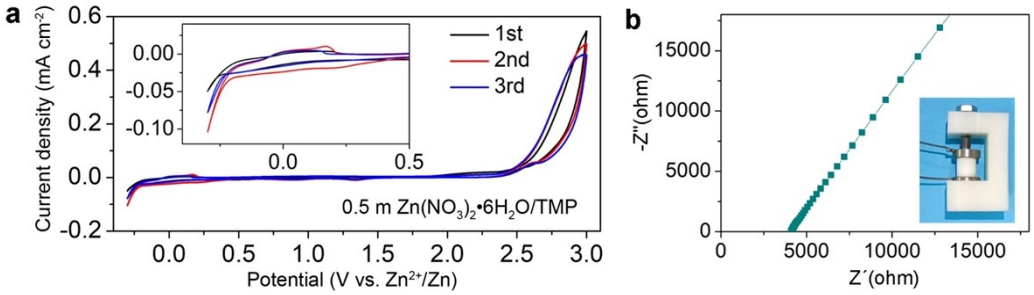

Fig. S3. (a) CV profiles of the Zn//Ti cell in the 0.5 m $Zn(NO_3)_2 \cdot 6H_2O$/TMP electrolyte at 1 mV s^{-1} from -0.3 to 3.0 V (vs. Zn^{2+}/Zn). (b) Nyquist plot of the 0.5 m $Zn(NO_3)_2 \cdot 6H_2O$/TMP electrolyte at room temperature. Inset is the photograph of a testing cell with a fully loading electrolyte.

The $Zn(NO_3)_2 \cdot 6H_2O$ based electrolyte exhibits a weak Zn^{2+} plating/stripping process due to its low conductivity and exhibits severe electrolyte decomposition occurring at 2.5 V. The ionic conductivity (σ) can be evaluated by the following equation: σ = L/RA,[S6,S7] where R represents the resistance (4048 Ω) according to the EIS measurement, L represents the length of the testing cell (1.0 cm), and A is the contact area between electrode and electrolyte in the testing cell (0.196 cm^{-2}). Accordingly, the ionic conductivity of 0.5 m $Zn(NO_3)_2 \cdot 6H_2O$/TMP is calculated to be 1.26 mS cm^{-1}.

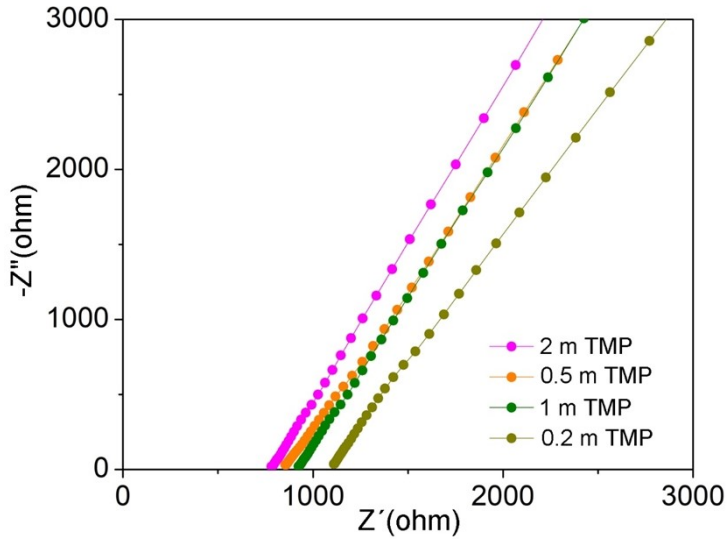

Fig. S4. Nyquist plot of the *x* m $Zn(ClO_4)_2 \cdot 6H_2O$/TMP electrolytes at room temperature (x = 0.2, 0.5, 1, and 2).

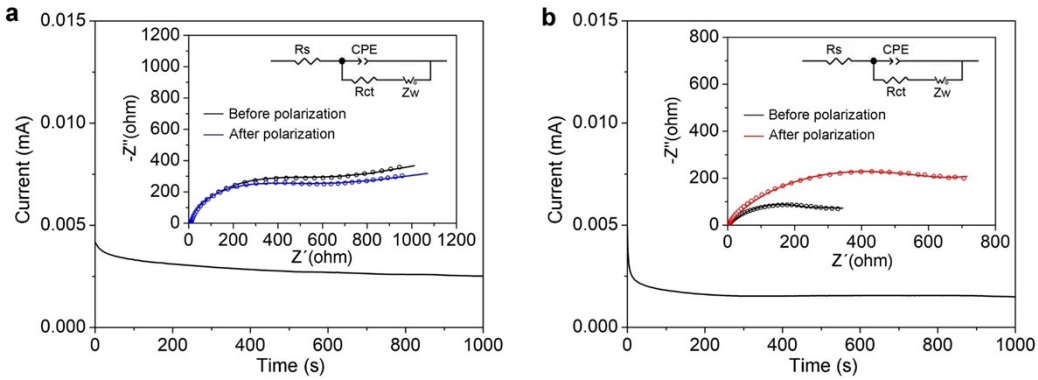

Fig. S5. Current-time plots of symmetric Zn//Zn cells in (a) 0.5 m TMP and (b) 0.5 m H_2O electrolytes following a constant polarization of 10 mV for 1000 s. The insets are the corresponding impedance spectra before and after polarization.

The Zn-ion transference number (t_{Zn}^{2+}) is estimated by the following equation[S6,S8]:

$$t_{Zn^{2+}} = \frac{I_s(\Delta V - I_0 R_0)}{I_0(\Delta V - I_s R_s)}$$

where ΔV is the constant polarization voltage applied (10 mV), I_0 and R_0 are the initial current and resistance, and I_s and R_s are the steady-state current and resistance, respectively. The I_0, I_s, R_0, and R_s for 0.5 m TMP are 4.18 μA, 2.51 μA, 700 Ω, 563 Ω, respectively. The I_0, I_s, R_0, and R_s for 0.5 m H_2O are 4.89 μA, 1.49 μA, 320 Ω, 720 Ω, respectively. Accordingly, the Zn^{2+} transference number for 0.5 m TMP and 0.5 m H_2O electrolytes are 0.49 and 0.28, respectively.

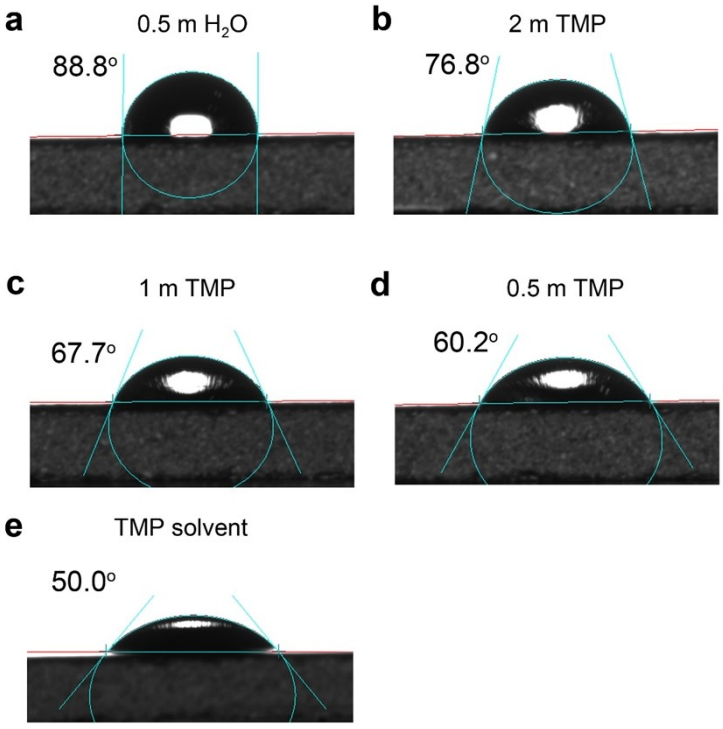

Fig. S6. Contact angle measurement of (a) 0.5 m H_2O, (b) 2 m TMP, (c) 1 m TMP, (d) 0.5 m TMP electrolytes and (e) TMP solvent on the Zn electrode.

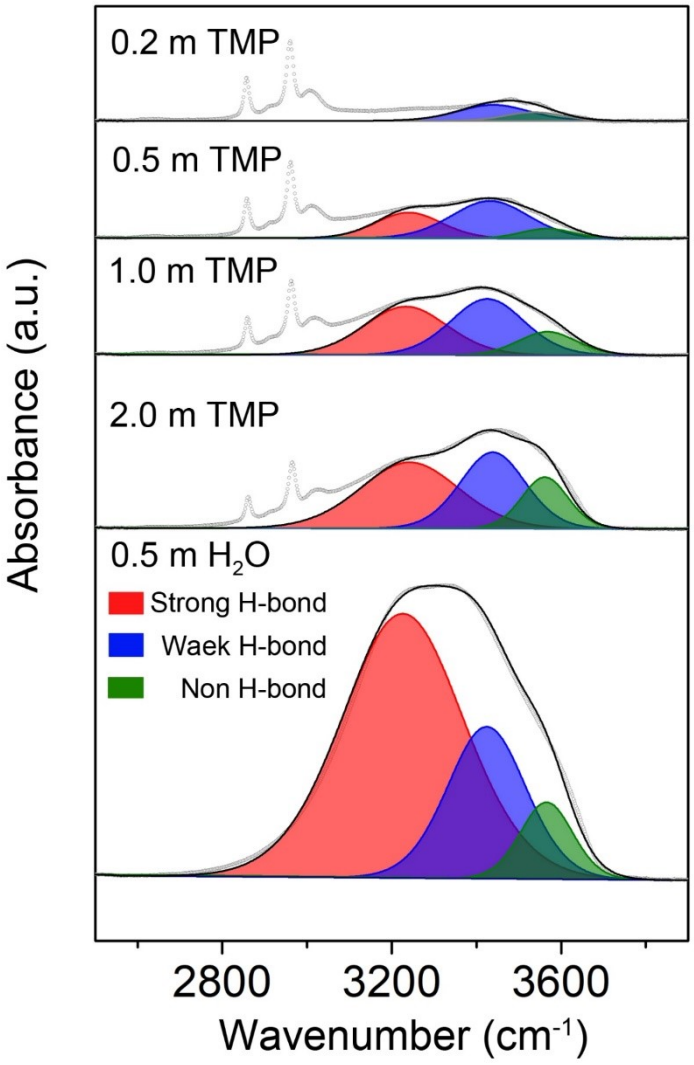

Fig. S7. FTIR spectra of various electrolytes with typically fitted curves representing three states of water molecules with different H-bonding environments (i.e., strong H-bond, weak H-bond, and non H-bond).

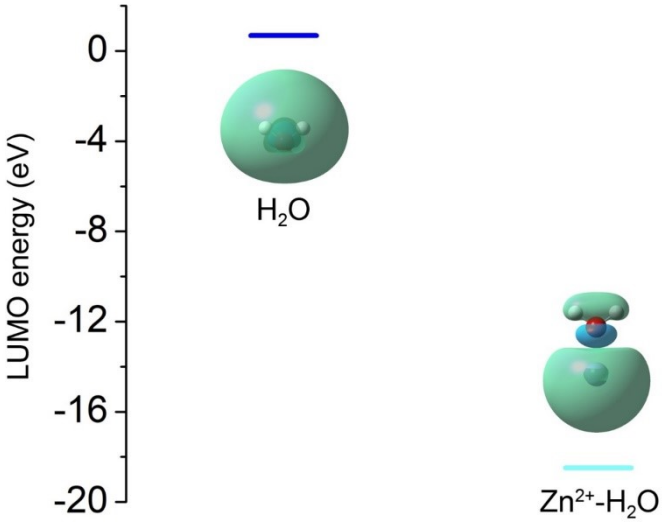

Fig. S8. LUMO energy levels with corresponding isosurfaces of free H_2O and solvating-H_2O (Zn^{2+}-H_2O). A lower LUMO energy level indicates a higher reductive activity.

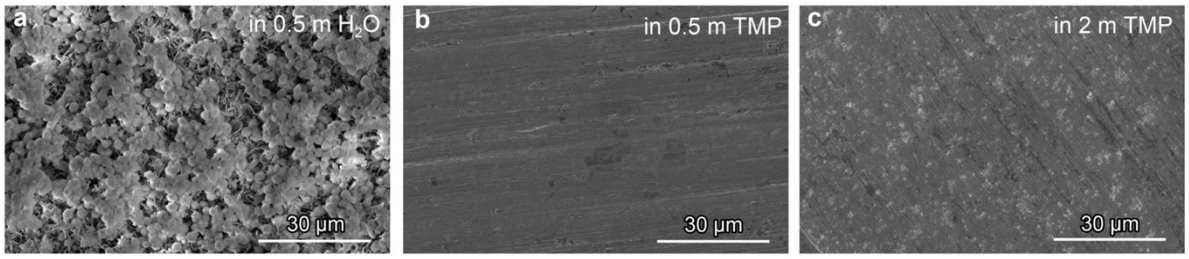

Fig. S9. Low-magnification SEM images of Zn electrodes after soaking in (a) 0.5 m H_2O, (b) 0.5 m TMP, and (c) 2 m TMP for 3 days.

Fig. S10. A digital photo of the 0.5 m TMP electrolyte containing 0.1 m $ZnCl_2$ salt after 30 min sonication.

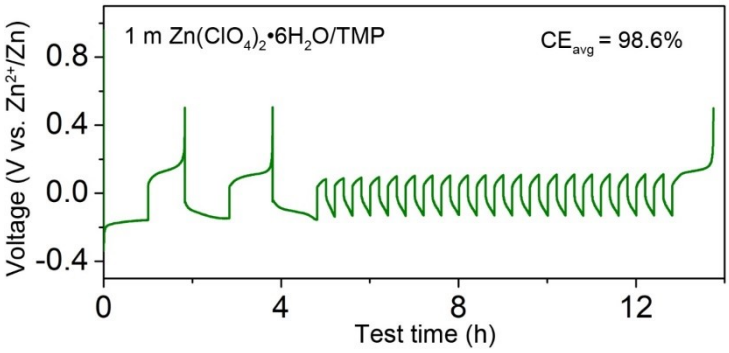

Fig. S11. Voltage profile of a Zn//Cu cell in 1 m TMP using a 'reservoir half-cell' method.

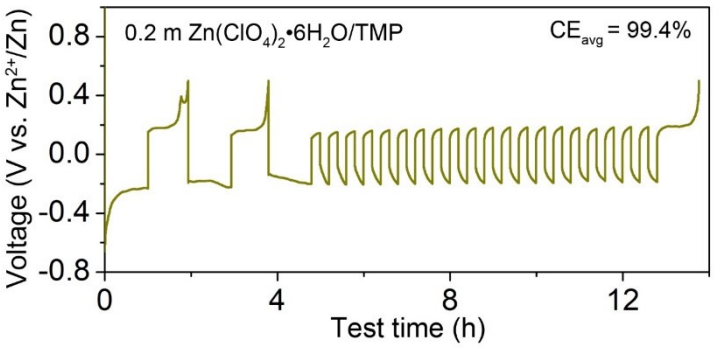

Fig. S12. Voltage profile of a Zn//Cu cell in 0.2 m TMP using a 'reservoir half-cell' method.

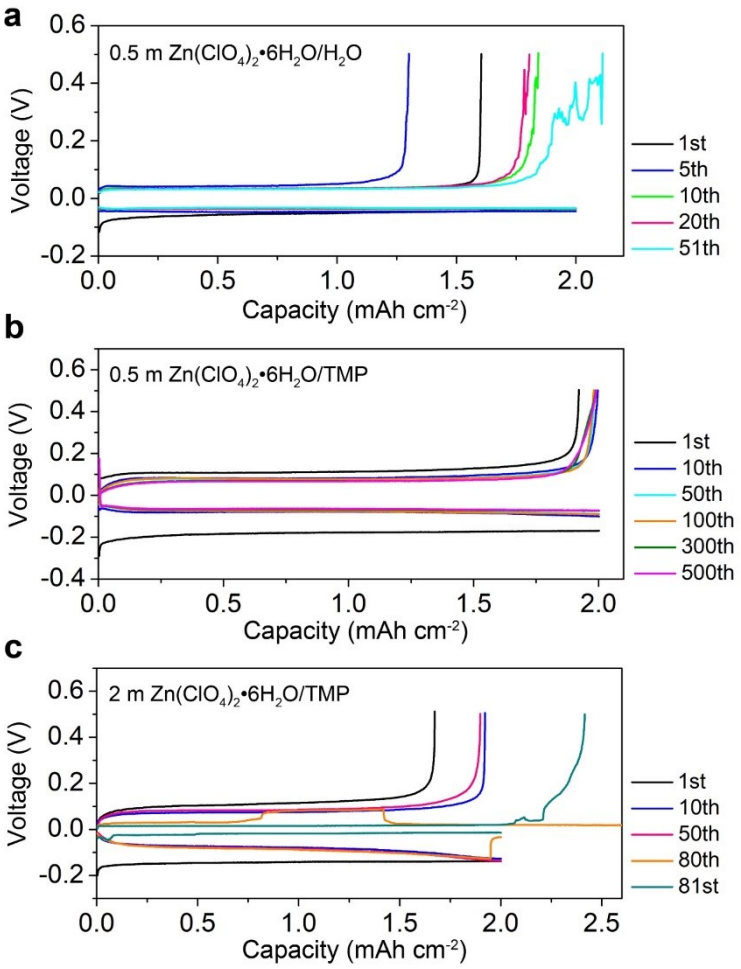

Fig. S13. Voltage profiles of Zn//Cu cells in (a) 0.5 m H_2O, (b) 0.5 m TMP, and (c) 2 m TMP at 2 mA cm^{-2} and 2 mAh cm^{-2}.

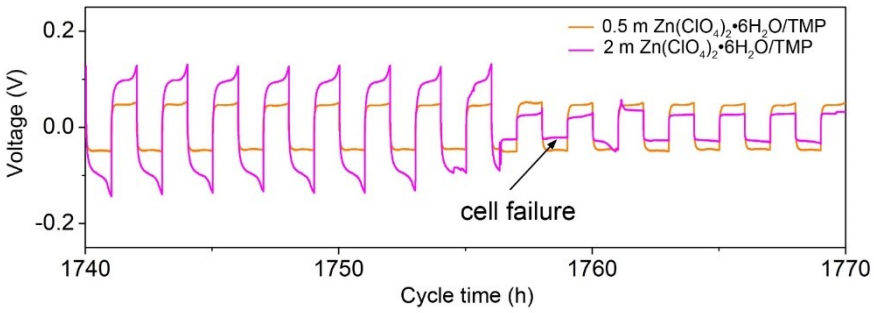

Fig. S14. Enlarged voltage profiles of Zn//Zn cells in 0.5 m and 2 m TMP at 1 mA cm^{-2} with 1 mAh cm^{-2}.

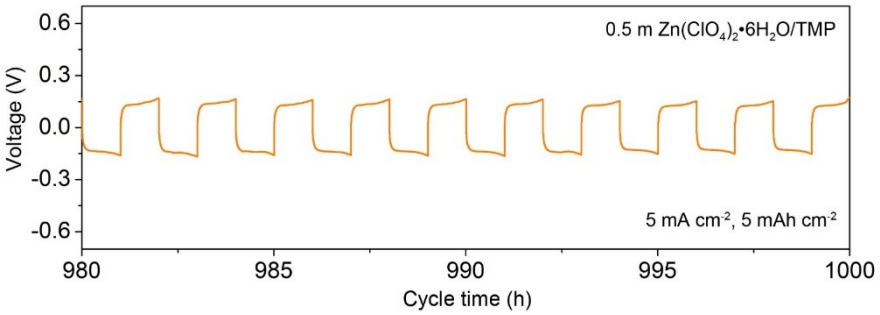

Fig. S15. Enlarged voltage profile of Zn//Zn cell in 0.5 m TMP at 5 mA cm^{-2} with 5 mAh cm^{-2}.

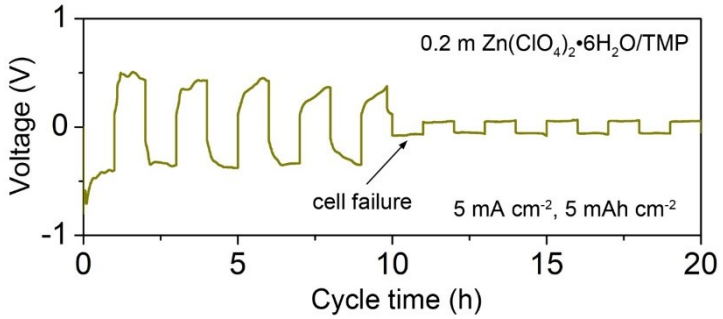

Fig. S16. Voltage profile of Zn//Zn cell in 0.2 m TMP at 5 mA cm^{-2} with 5 mAh cm^{-2}.

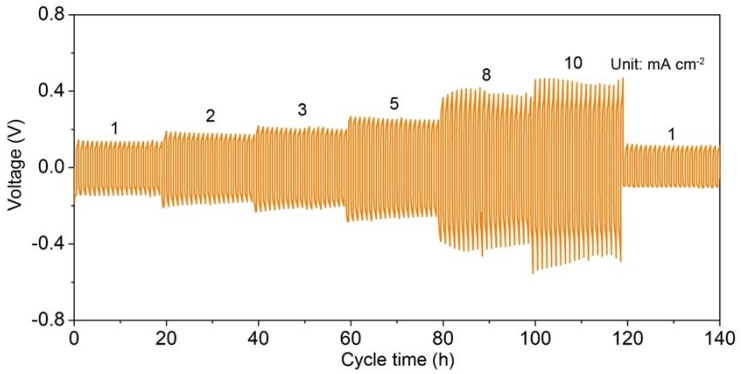

Fig. S17. Rate performance of Zn//Zn cell in 0.5 m TMP at various current densities with a plating/stripping time of 0.5 h.

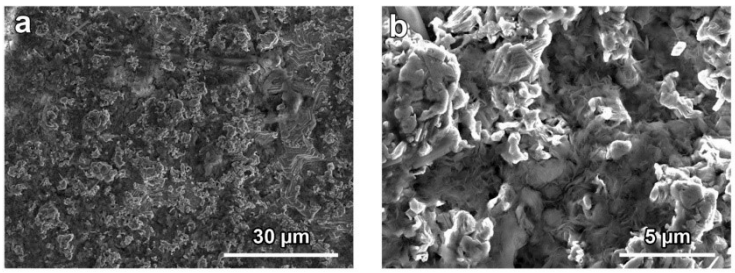

Fig. S18. (a) Low-magnification and (b) high-magnification SEM images of the Zn electrode in 2 m TMP electrolyte after 100 cycles at 1 mA cm^{-2}.

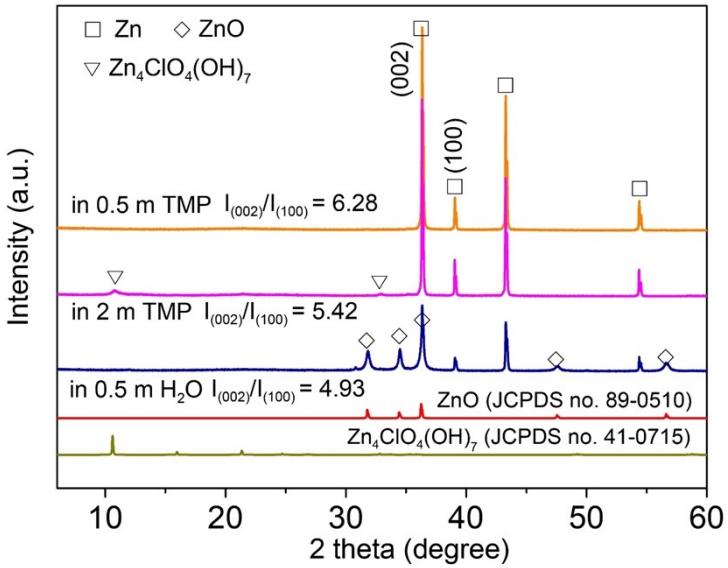

Fig. S19. XRD patterns of the Zn electrodes after 100 cycles in 0.5 m H_2O, 0.5 m TMP, and 2 m TMP electrolytes.

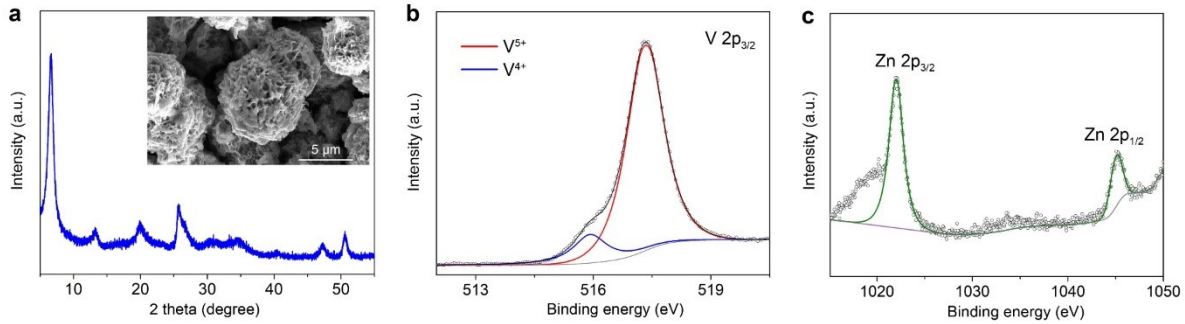

Fig. S20. (a) XRD pattern and SEM image (inset) of the as-prepared ZVO cathode. XPS spectra of (b) V 2p and (c) Zn 2p regions. The average V valance in the cathode material is calculated to be around 4.87, based on the areal ratio of V^{5+} : V^{4+} XPS signal. Thus, the *x* value in the as-prepared $Zn_xV_2O_5{\cdot}nH_2O$ is around 0.13.

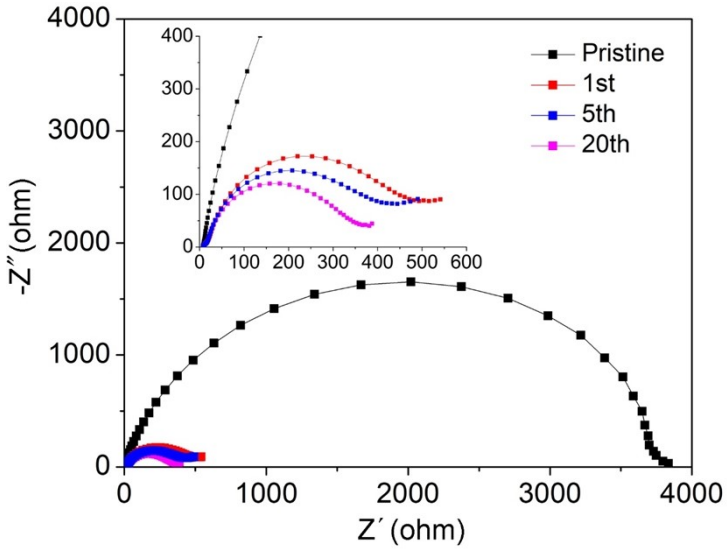

Fig. S21. EIS spectra of the Zn//0.5 m TMP//ZVO battery at selected cycles.

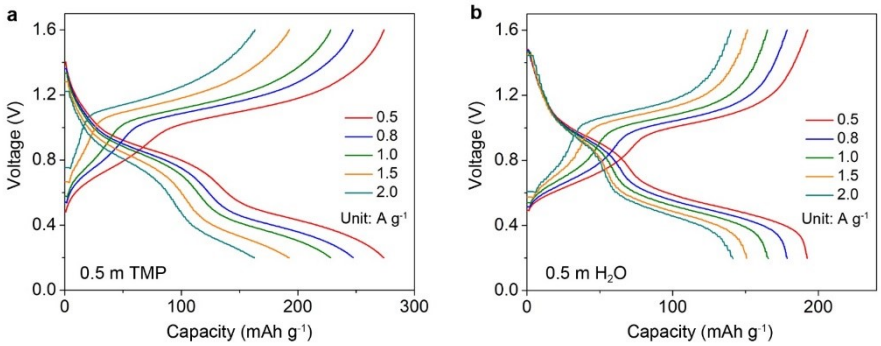

Fig. S22. Voltage profiles of the Zn//ZVO full batteries in (a) 0.5 m TMP and (b) 0.5 m H_2O at various current densities.

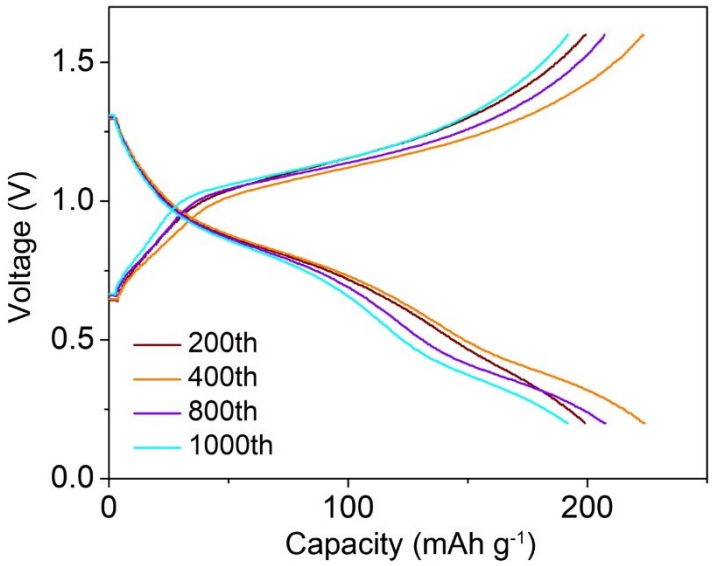

Fig. S23. Selected voltage profiles of the Zn//ZVO full battery in 0.5 m TMP at 1 A g^{-1}.

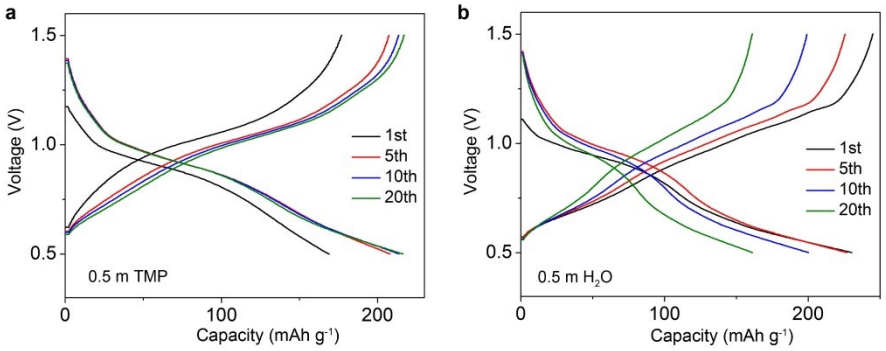

Fig. S24. Voltage profiles of the Zn//ZVO full battery in (a) 0.5 m TMP and (b) 0.5 m H_2O at 0.5 A g^{-1} under a high operating temperature of 50 ºC.

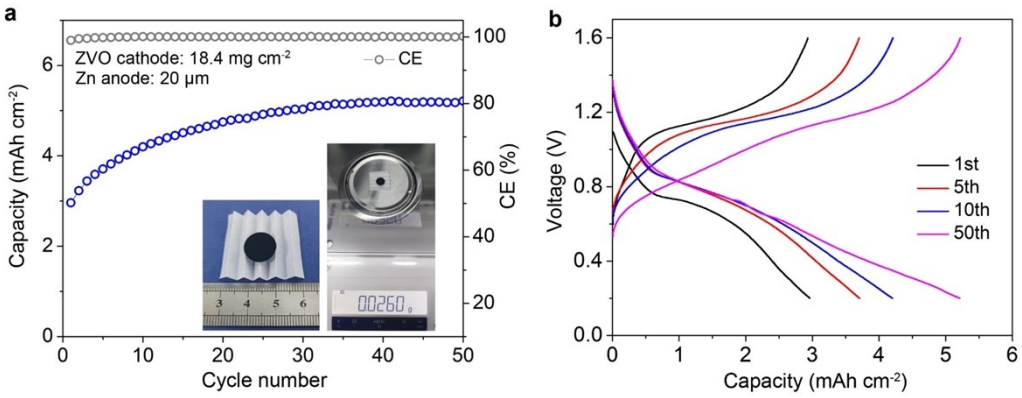

Fig. S25. (a) Cycling stability at 0.1 A $g_{cathode}^{-1}$ and (b) voltage curves of full battery coupling 20-μm-thick Zn anode with high mass loading ZVO cathode (18.4 mg cm^{-2}). Insets show the digital photos of the binder-free ZVO electrode with a high mass loading. The mass ratio of ZVO:CNTs in the electrode is 8:2. The mass and diameter of ZVO electrode are 26.0 mg and 1.13 cm^{-2}, respectively. The mass loading of VOH was calculated to be 18.4 mg cm^{-2}.

Table S1. The composition of ion/molecules in different electrolytes for MD simulations.

Electrolyte	**Zn^{2+}**	**ClO_4^-**	**TMP**	**H_2O**
0.5 m $Zn(ClO_4)_2 \cdot 6H_2O$ in H_2O	50	100	-	5850
2 m $Zn(ClO_4)_2 \cdot 6H_2O$ in TMP	50	100	179	300
0.5 m $Zn(ClO_4)_2 \cdot 6H_2O$ in TMP	50	100	714	300

Table S2. Comparison of electrochemical performances of this work with previously reported asymmetric Zn-based cells.

Electrode	Electrolyte (M: mol/L m : mol/kg)	Asymmetric Zn-based cells			Ref.
		Current density (mA cm^{-2})/Capacity (mAh cm^{-2})	Initial CE	Average CE	
Zn foil (50 μm)	**0.5 m $Zn(ClO_4)_2·6H_2O$/TMP**	**2/2**	**95.9%**	**99.5% after 500 cycles**	**This work**
Zn foil (100 μm)	4 m $Zn(BF_4)_2·4.5H_2O$/ethylene glycol	1/0.5	~65%	99.4% after 400 cycles	S6
Zn foil (-- μm)	$Zn(ClO_4)_2·6H_2O$/succinonitrile (molar ratio: 1:8)	0.5/0.5	~85%	98.4% after 90 cycles	S9
Zn foil (-- μm)	$Zn(ClO_4)_2·6H_2O$/sulfolane (molar ratio: 1:6)	0.5/0.5	~57%	98% after 100 cycles	S10
Zn foil (-- μm)	$ZnCl_2$/acetamide+H_2O (molar ratio: 1:3:1)	0.1/0.025	~78%	98.0% after 1000 cycles	S11
Zn foil (-- μm)	0.5 m $Zn(ClO_4)_2$+18 m $NaClO_4$	0.4/0.4	~78%	98.2% after 100 cycles	S12
Zn foil (-- μm)	0.5 M $Zn(OTf)_2$/trimethyl phosphate+dimethyl carbonate (volume ratio: 1:1)	1/0.5	~97%	99.15% after 300 cycles	S13
Zn foil (-- μm)	1.3 m $ZnCl_2/H_2O$+dimethyl sulfoxide (volume ratio: 4.3:1)	1/0.5	~94%	99.5% after 400 cycles	S14
Zn foil (100 μm)	1 m $Zn(TFSI)_2$+20 m LiTFSI	1/0.167	~98.0%	99.7% after 200 cycles	S15
Zn foil (80 μm)	$ZnCl_2+Zn(OAc)_2·2H_2O/H_2O$ (molar ratio: 10:6:18.5)	0.2/0.2	~81%	99.59% after 500 cycles	S16
Zn foil (100 μm)	1 M $ZnSO_4$+10 mM glucose	1/0.5	~69%	97.2% after 200 cycles	S17

Zn foil (150 μm-250 μm)	2 M $ZnSO_4$+0.5 g L^{-1} benzyltrimethylammonium chloride	0.5/1	~60%	99.0% after 200 cycles	S18
Zn foil (80 μm)	0.5 M $ZnCl_2$+1 M triethylmethylammonium chloride	1/0.5	~71%	97.7% after 750 cycles	S19

Supplementary References

[S1] Q. Liu, Y. Wang, X. Hong, R. Zhou, Z. Hou and B. Zhang, *Adv. Energy Mater.*, 2022, **12**, 2200318.

[S2] H. J. C. Berendsen, D. van der Spoel and R. van Drunen, *Comp. Phys. Comm.*, 1995, **91**, 43-56.

[S3] Y. Duan, C. Wu, S. Chowdhury, M. C. Lee, G. Xiong, W. Zhang, R. Yang, P. Cieplak, R. Luo, T. Lee, J. Caldwell, J. Wang and P. Kollman, *J. Comput. Chem.*, 2003, **24**, 1999-2012.

[S4] A. W. S. da Silva and W. F. Vranken, *BMC Res. Notes*, 2012, **5**, 367.

[S5] W. Humphrey, A. Dalke and K. Schulten, *J. Mol. Graph.*, 1996, **14**, 33-38.

[S6] D. Han, C. Cui, K. Zhang, Z. Wang, J. Gao, Y. Guo, Z. Zhang, S. Wu, L. Yin, Z. Weng, F. Kang and Q. Yang, *Nat. Sustain.*, 2022, **5**, 205-213.

[S7] G. Ma, L. Miao, Y. Dong, W. Yuan, X. Nie, S. Di, Y. Wang, L. Wang and N. Zhang, *Energy Storage Mater.*, 2022, **47**, 203-210.

[S8] H. Qiu, X. Du, J. Zhao, Y. Wang, J. Ju, Z. Chen, Z. Hu, D. Yan, X. Zhou and G. Cui, *Nat. Commun.*, 2019, **10**, 5374.

[S9] W. Yang, X. Du, J. Zhao, Z. Chen, J. Li, J. Xie, Y. Zhang, Z. Cui, Q. Kong, Z. Zhao, C. Wang, Q. Zhang and G. Cui, *Joule*, 2020, **4**, 1557-1574.

[S10] X. Lin, G. Zhou, M. J. Robson, J. Yu, S. C. T. Kwok and F. Ciucci, *Adv. Funct. Mater.*, 2022, **32**, 2109322.

[S11] J. Shi, T. Sun, J. Bao, S. Zheng, H. Du, L. Li, X. Yuan, T. Ma and Z. Tao, *Adv. Funct. Mater.*, 2021, **31**, 2102035.

[S12] Y. Zhu, J. Yin, X. Zheng, A.-H. Emwas, Y. Lei, O. F. Mohammed, Y. Cuice and H. N. Alshareef, *Energy Environ. Sci.*, 2021, **14**, 4463-4473.

[S13] A. Naveed, H. Yang, Y. Shao, J. Yang, N. Yanna, J. Liu, S. Shi, L. Zhang, A. Ye, B. He and J. Wang, *Adv. Mater.*, 2019, **31**, 1900668.

[S14] L. Cao, D. Li, E. Hu, J. Xu, T. Deng, L. Ma, Y. Wang, X.-Q. Yang and C. Wang, *J. Am. Chem. Soc.*, 2020, **142**, 21404-21409.

[S15] F. Wang, O. Borodin, T. Gao, X. Fan, W. Sun, F. Han, A. Faraone, J. A. Dura, K. Xu and C. Wang, *Nat. Mater.*, 2018, **17**, 543-549.

[S16] M. Yang, J. Zhu, S. Bi, R. Wang and Z. Niu, *Adv. Mater.*, 2022, **34**, 2201744.

[S17] P. Sun, L. Ma, W. Zhou, M. Qiu, Z. Wang, D. Chao and W. Mai, *Angew. Chem. Int. Ed.*, 2021, **60**, 18247-18255.

[S18] K. Guan, L. Tao, R. Yang, H. Zhang, N. Wang, H. Wan, J. Cui, J. Zhang, H. Wang and H. Wang, *Adv. Energy Mater.*, 2022, **12**, 2103557.

[S19] R. Yao, L. Qian, Y. Sui, G. Zhao, R. Guo, S. Hu, P. Liu, H. Zhu, F. Wang, C. Zhi and C. Yang, *Adv. Energy Mater.*, 2022, **12**, 2102780.